Simplified Reflection-Based Calibration for a Multistatic Microwave Imaging System

Simplified Reflection-Based Calibration for a Multistatic Microwave Imaging System

Alex R. Masaquiza-Caiza, Martina Gugliermino, David O. Rodriguez-Duarte, Francesca Vipiana
Dept. Electronics and Telecommunications, Politecnico di Torino, Torino, Italy
francesca.vipiana@polito.it

***Abstract*—This work presents a simplified calibration procedure for multistatic microwave imaging systems that uses both the time-domain reflection signatures of the entire system and an extended two-port calibration in an auxiliary channel to correct temporal drifts and align the measurement reference planes with the inversion kernel. This approach substantially reduces the experimental burden and complexity of a standard full calibration and allows for continuous calibration without hardware setup intervention during measuring campaigns. Its performance is experimentally tested on a single-ring eight-antenna system, with two groups of four antennas, each connected to a one-pole-four-through RF switch, and a simplified cylindrical phantom that mimics the average dielectric properties of human head tissues. For imaging, a multi-frequency bi-focusing algorithm is employed, yielding a noticeable improvement over the uncalibrated case, as evaluated by various metrics.**

***Index Terms*—Calibration, microwave imaging**

I. Introduction

Accurate calibration is required for microwave imaging (MWI) algorithms, as image quality depends, among other factors, on the consistent alignment of the measurement and inversion kernel. That correspondence ensures that the phase center of the measurement antennas consistently corresponds to the ones of the MWI algorithms. When the inversion kernel uses a full-wave electromagnetic antenna model [1], this information is inherently included, and the calibration becomes less critical. But for MWI algorithms, such as the confocal-based ones [2], where this information is not explicitly included, the calibration becomes more important. In practice, this alignment is non-trivial for systems whose channels have different electrical lengths or employ electrically complex antennas.

To address these challenges, some calibration methods for multistatic systems have been proposed, including techniques that model the antennas and field propagation as two-port networks, followed by de-embedding; extrapolation-based methods to extend a two-port to a multi-port calibration; cavity-based methods using the two-port unknown-thru calibration; and phase-based methods that compensates the channel-dependent electrical length variations [3], [4], [5], [6].

In this work, we introduce a simplified calibration method that eliminates the need for a standard n-port calibration, which requires at least $4n-1$ measurements [7], where n is the number of antennas. This calibration uses an auxiliary channel to map the measurement calibration plane to the inversion kernel reference plane. It allows for an on-demand recalibration of the MWI system without hardware changes between measurements, similar to a calibration refresh module [8]. The method is experimentally validated in an MWI system with a sparse-view circular eight-antenna array.

II. Experimental Setup

This section introduces the experimental setup used to validate the calibration procedure. As shown in Fig. 1, it includes a single-ring antenna array, two one-pole-eight-thru solid-state RF switches (Sw_A and Sw_B) [9], though, just five channels are used at each, a Keysight P5003B Vector Network Analyzer (VNA) [10], and an electronic calibration module (E-cal) [11]. All coaxial cables connecting the hardware have equivalent electrical lengths. On each RF switch, one channel is reserved for the E-Cal, which allows full calibration of a reference channel without disturbing the system. The antennas are printed monopoles on a thin FR4 substrate with a slab of lossy matching medium (Ant-MM), evenly distributed around the phantom and operating

This work was supported in part by the research project "3BAtwin" funded by Horizon EU FP (101159623), and the research project "MedWaveImage - Microwave imaging technology transfer to innovate the medical sector", funded by Interreg Central Europe (CE0200670) This manuscript reflects only the authors' views and opinions, neither the European Union nor the European Commission can be considered responsible for them.

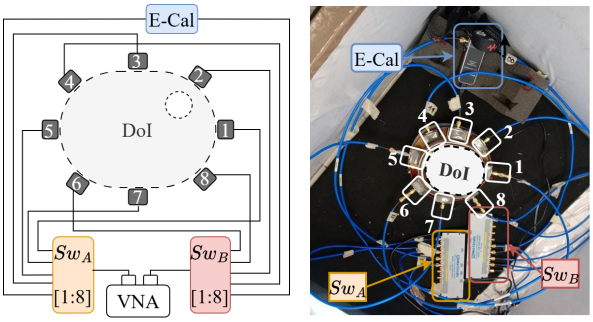

(a) (b)

Fig. 1. Multistatic MWI system setup: (a) diagram of the MWI system; (b) implemented MWI system.

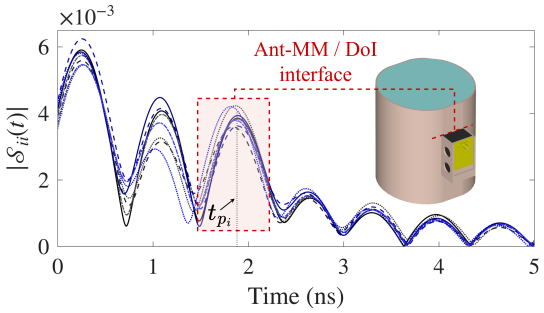

Fig. 2. Time-domain $\mathcal{S}_{ii}(t)$, $i \in (1, ..., 8)$; dashed region encloses the reflection produced by the Ant-MM/DoI interface.

in the 0.9–1.8 GHz band, optimized to operate with a phantom such as the one used here. Further details on the antennas are found in [4].

The phantom is a 1 mm-thick plastic container filled with an ad hoc liquid mixture of water, alcohol, and salt, whose dielectric properties approximate those of average brain tissue with a relative permittivity and conductivity of approximately 45, and 0.8 S/m, respectively, at 1 GHz, [1]. The imaging target is a 1 cm-radius teflon cylinder placed at different positions.

III. Reflection-based Calibration

The calibration procedure consists of four steps. In the first step (I), we perform a standard two-port calibration on two reference channels using the E-cal, then extrapolate to the others, following the approach in [4]. This assumes that the signal paths from the VNA to each antenna port are electrically equivalent to the reference channel calibrated with the E-cal. Next, in step (II), we measure the multistatic scattering parameters in a known scenario. Then, in step (III), the reflection coefficients are converted from frequency-domain to time-domain to determine the round-trip delay and phase from the measurement calibration plane, i.e., the antenna ports, to a new reference plane. This new plane is the interface between the Ant-MM and the external boundary phantom, which also defines the boundary of the domain of imaging (DoI), hereafter referred to as the Ant-MM/DoI interface. The reflection responses are shown in Fig. 2, each i antenna has multiple peaks. The first ones are attributed to reflections from the multilayer antenna structure, and the third one (inside the red-dashed region) corresponds to the Ant-MM/DoI interface. Finally, in step (IV), we apply the calibration to align each channel's reference plane with the corresponding Ant/DoI interface. From the signals in Fig. 2, for each i antenna, the corresponding peak at time t_{p_i} is isolated using the time-domain gating technique, and the associated phase contribution in the frequency-domain corresponds to propagation from the antenna port to the corresponding Ant-MM/DoI interface. As is shown in [6], this phase information can be use to synthetically translate the measurement reference plane as a frequency-dependent phase compensation or, as in this work, via a equivalent time shift in the time-domain scattered signals to suppress the effect of propagation within the antenna structure itself.

Here, $\mathcal{S}_{ij}(t)$ and $S_{ij}(f)$ are the time- and frequency-domain representations of the scattered responses, respectively, and t_{p_i} and t_{p_j} the round-trip propagation delays from the i, and j antenna ports to their Ant-MM/DoI interface. Thus, the measurement calibration plane is translated to the Ant-MM/DoI interface as:

$$\mathcal{S}_{ij}^{\text{cal}}(t) = \mathcal{S}_{ij}(t + (t_{p_i}/2 + t_{p_j}/2)), \tag{1}$$

where $\mathcal{S}_{ij}^{\text{cal}}(t)$ is the calibrated scattering response in the time-domain, or the equivalent $\mathbf{S}_{ij}^{\text{cal}}$ in the frequency-domain.

IV. Experimental Results

To validate the calibration procedure, MWI reconstructions are obtained using the Multi-frequency Bi-focusing algorithm [2]. The normalized reconstructed intensity maps are shown in Fig. 3. The target is located at two different positions (dashed white contours), referred to as Pos_1 and Pos_2 in Fig. 3(a-c) and Fig. 3(b-d), respectively. In the uncalibrated reconstructions, the antenna positions provided to the MWI inversion kernel correspond to the calibration plane of the measurements, i.e., the antenna ports. However, even if the physical antenna port location in space is known, the electrically complex structure of the

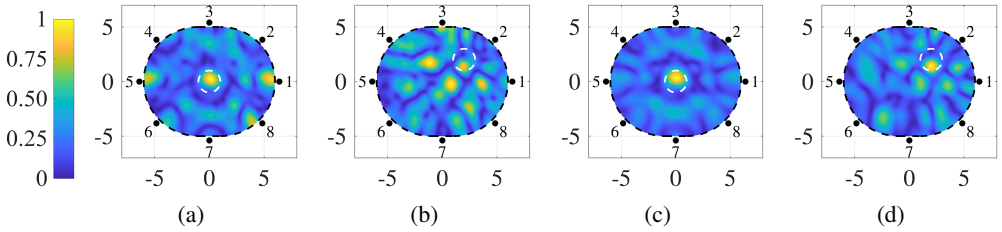

Fig. 3. Normalized MWI reconstructions: (a–b) non-calibrated, (c–d) calibrated; (a) and (c) corresponds to Pos_1, (b) and (d) corresponds to Pos_2. Dimensions are in cm. The white dashed circumferences indicate the target shape and location.

TABLE I
RECONSTRUCTION PERFORMANCE METRICS

	Target position	IoU	DSC	S-BM	SSIM
Non calibrated	Pos_1	0.232	0.376	0.928	0.910
	Pos_2	0.072	0.134	0.753	0.869
Calibrated	Pos_1	0.570	0.726	0.835	0.968
	Pos_2	0.205	0.340	0.860	0.937

antennas introduces phase inconsistencies between the measurement and the MWI algorithm reference planes. As a result, artifacts appear in the reconstructions. After calibration, the reference plane of both the scattering data and the MWI algorithm corresponds to each other, i.e., the reference plane for both is the Ant-MM/DoI interface. As a result, the target is correctly localized, and the background artifacts are significantly reduced.

The quality of the MWI reconstructions are evaluated using the following metrics: intersection over union (IoU), dice similarity coefficient (DSC) [12], a size-based metric (S-BM) proposed in [13], and the structural similarity index (SSIM). For that, the ground truth of the expected reconstruction is compared with the reconstructed binarized intensity maps, where the values above 0.561 ($\approx -5\,\text{dB}$) are set to 1, and the values below are set to 0. A metric value of 0 indicates a complete mismatch between the reconstructed and expected intensity map, and 1 indicates a perfect correspondence. Table I summarizes the results, showing that MWI reconstructions with calibrated data locate the target more accurately than those with non-calibrated data.

V. CONCLUSIONS

The work has presented a simplified reflection-based calibration procedure for a multistatic MWI to effectively align the measurement reference plane with the kernel inversion of MWI algorithms, exploiting the time-domain reflection signatures. This method reduces the complexity and time of a full standard calibration that requires at least $4n - 1$ standard measurements, with n the number of antennas. Moreover, it uses an auxiliary channel with an E-cal module that allows recalibration between measurements without the need for any modification in the hardware. Experimental results confirm that the calibration improves the MWI reconstructions and reduces background artifacts.

REFERENCES

[1] D. O. Rodriguez-Duarte and et al., "Experimental assessment of real-time brain stroke monitoring via a microwave imaging scanner," *IEEE Open Journal of Antennas and Propagation*, vol. 3, pp. 824–835, 2022.

[2] L. Jofre et al., "UWB Short-Range Bifocusing Tomographic Imaging," *IEEE Transactions on Instrumentation and Measurement*, vol. 57, no. 11, pp. 2414–2420, 2008.

[3] S. Cathers, J. LoVetri, I. Jeffrey, and C. Gilmore, "Electromagnetic imaging system calibration with 2-port error models," *IEEE Open Journal of Antennas and Propagation*, vol. 4, pp. 1142–1153, 2023.

[4] M. Gugliermino et al., "On the use of an electro-mechanical and a solid-state switching matrix for a portable microwave-based brain stroke scanner," *IEEE Antennas and Wireless Propagation Letters*, 2024.

[5] M. Haynes, J. Stang, and M. Moghaddam, "Real-time microwave imaging of differential temperature for thermal therapy monitoring," *IEEE Transactions on Biomedical Engineering*, vol. 61, no. 6, pp. 1787–1797, 2014.

[6] H. Tabata, M. R. Asakawa, and S. Yamaguchi, "Accurate phase calibration of multistatic imaging system for medical and industrial applications," *Applied Sciences*, vol. 14, no. 22, p. 10 671, 2024.

[7] V. Teppati, A. Ferrero, and M. Sayed, "Multiport s-parameters measurement methods," in *Modern RF and Microwave Measurement Techniques*, A. Ferrero and M. Sayed, Eds., Cambridge University Press, 2013, pp. 219–240.

[8] *Keysight technologies 855xxa/b series calpods and 85523b calpod controller – performance characteristics*, https://www.keysight.com/us/en/assets/9921-01890/reference-guides/855xxA-B-Series-CalPods-and-85523-CalPod-Controller-Performance-Characteristics.pdf, 2013.

[9] Mini-Circuits, *Usb-1sp8t-852h solid-state switch datasheet*, Mini-Circuits, Brooklyn, NY, USA, 2023. [Online]. Available: https://www.minicircuits.com/pdfs/USB-1SP8T-852H.pdf.

[10] *Streamline series vector network analyzer*, Available at https://www.keysight.com/jp/ja/assets/3121-1235/data-sheets/Streamline-Series-Vector-Network-Analyzer-B-models.pdf.

[11] *Keysight datasheet*, Available at https://www.keysight.com/us/en/product/N7551A/electronic-calibration-module-ecal-dc-6-5-ghz-2-port.html.

[12] K. H. Zou et al., "Statistical validation of image segmentation quality based on a spatial overlap index1: Scientific reports," *Academic radiology*, vol. 11, no. 2, pp. 178–189, 2004.

[13] F. Xue, L. Guo, A. Bialkowski, and A. M. Abbosh, "Integrated boundary-overlap-size metric for local assessment of deep learning methods in medical microwave imaging," *IEEE Journal of Electromagnetics, RF and Microwaves in Medicine and Biology*, vol. 9, no. 2, pp. 229–239, 2025.